European Radiology (2022) 32:8649–8658
https://doi.org/10.1007/s00330-022-08908-y

MAGNETIC RESONANCE

Gray matter microstructural alterations in manganese-exposed welders: a preliminary neuroimaging study

Jiayu Wu[1] · Qiaoying Zhang[1] · Pengfeng Sun[1] · Hong Zhang[1] · Ming Gao[1] · Mingyue Ma[1] · Yan Dong[1] · Peng Liu[2,3] · Xiaoping Wu[1]

Received: 21 January 2022 / Revised: 13 April 2022 / Accepted: 23 May 2022 / Published online: 23 June 2022

Abstract

Objectives Chronic occupational manganese (Mn) exposure is characterized by motor and cognitive dysfunction. This study aimed to investigate structural abnormalities in Mn-exposed welders compared to healthy controls (HCs).

Methods Thirty-five HCs and forty Mn-exposed welders underwent magnetic resonance imaging (MRI) scans in this study. Based on T1-weighted MRI, the voxel-based morphometry (VBM), structural covariance, and receiver operating characteristic (ROC) curve were applied to examine whole-brain structural changes in Mn-exposed welders.

Results Compared to HCs, Mn-exposed welders had altered gray matter volume (GMV) mainly in the medial prefrontal cortex, lentiform nucleus, hippocampus, and parahippocampus. ROC analysis indicated the potential highest classification power of the hippocampus/parahippocampus. Moreover, distinct structural covariance patterns in the two groups were associated with regions, mainly including the thalamus, insula, amygdala, sensorimotor area, and middle temporal gyrus. No significant relationships were found between the findings and clinical characteristics.

Conclusions Our findings showed Mn-exposed welders had changed GMV and structural covariance patterns in some regions, which implicated in motivative response, cognitive control, and emotional regulation. These results might provide preliminary evidence for understanding the pathophysiology of Mn overexposure.

Key Points

- *Chronic Mn exposure might be related to abnormal brain structural neural mechanisms.*
- *Mn-exposed welders had morphological changes in brain regions implicated in emotional modulation, cognitive control, and motor-related response.*
- *Altered gray matter volume in the hippocampus/parahippocampus and putamen might serve as potential biomarkers for Mn overexposure.*

Keywords Manganese exposure · Gray matter volume · Structural covariance · Magnetic resonance imaging

Abbreviations

AUC	Area under the curve
CI	Confidence interval
FDR	False discovery rate
GMV	Gray matter volume
HC	Healthy control
Mn	Manganese
MNI	Montreal Neurological Institute
MPFC	Medial prefrontal cortex
MRI	Magnetic resonance imaging

✉ Peng Liu
liupengphd@gmail.com

✉ Xiaoping Wu
szping518@163.com

[1] Department of Radiology, The Affiliated Xi'an Central Hospital of Xi'an Jiaotong University, Xi'an, China

[2] Life Science Research Center, School of Life Science and Technology, Xidian University, Xi'an 710071, Shaanxi, China

[3] Engineering Research Center of Molecular and Neuro Imaging Ministry of Education, School of Life Science and Technology, Xidian University, Xi'an, Shaanxi, China

MTG Middle temporal gyrus
ROC Receiver operating characteristic
ROI Region of interest
SMA Supplemental motor area
VBM Voxel-based morphometry

Introduction

Manganese (Mn) is an essential metal for maintaining human health and one of the most abundant elements in the world [1]. Exposure to high levels of Mn most occurs through inhalation from industrial sources and may lead to Mn neurotoxicity, which resembles idiopathic Parkinson's disease in its clinical characteristics [2]. Mn-exposed welders are reported to accompany abnormalities in motor, cognition, and emotion [3]. Meanwhile, chronic Mn exposure has posed a considerable economic burden to the individual and socially in the quality of life and work productivity. However, the pathophysiology of Mn neurotoxicity among Mn-exposed welders is not fully understood.

There are certain sites of Mn concentration like the pallidum, striatum, hippocampus, substantia nigra, and olfactory bulb reported in studies [4]. Recently, advance magnetic resonance imaging (MRI) techniques have been used to examine brain structural and functional abnormalities among Mn-exposed welders. For instance, Mn-induced mean diffusivity values increase was reported in the hippocampus, and the changes were associated with long-term cumulative Mn-exposure [5]. Another diffusion tensor imaging study investigated differences in white matter integrity and revealed Mn-exposed welders had a reduction of fractional anisotropy in the corpus callosum and frontal white matter compared to HCs [6]. In addition, task-based functional MRI detected increased brain activity in working memory and executive networks in Mn-exposed welders [3, 7]. Taken together, these studies indicate that abnormal brain neural system processing may be a relevant pathophysiologic mechanism in chronic Mn overexposure. However, studies on structural alterations of GMV in Mn-exposed welders are still limited.

Structural MRI provides unique brain microstructural properties information and has been widely used to capture the spatial patterns of key brain regions atrophy in patients with various disorders [8–11]. VBM is an advanced topological structure analysis technique, which involves a voxel-wise comparison of the local concentration of gray matter between two groups [12]. Structural covariance patterns closely mirror coordinated neurodevelopment patterns, and that covariance is associated with structural connectivity [13]. Previous studies revealed that structural covariance computed stable connectivity features and provided biomarkers of disease and treatment response in neurodevelopmental or connectivity disorders such as schizophrenia [14], Parkinson's disease [15], lifelong premature ejaculation [16], and ulcerative colitis [17]. Hence, it would be potentially worthy to combine VBM and structural covariance analysis to examine altered brain structural plasticity in Mn-exposed welders.

Thereby, the aims of this study were as follows: (i) to explore possible group differences in GMV between the Mn-exposed welders and age-matched HCs by VBM analysis; (ii) to investigate structural covariance patterns in ROIs in two groups by seed-based analysis; and (iii) to assess relationships between the changed GMV and clinical characteristics of Mn-exposure. Here, we hypothesized that (i) compared to HCs, Mn-exposed welders might have changed GMV in brain regions associated with motivation and cognition; (ii) Mn-exposed welders and HCs group might exhibit distinct structural covariance patterns; (iii) Mn-exposed welders might have correlations between the changed GMV and clinical characteristics.

Materials and methods

Ethics statement

The present study was conducted by the Xi'an Central Hospital affiliated to Xi'an Jiaotong University. Each subject was informed of the whole experiment procedure and signed a written informed consent prior to the study. The study was in accordance with the Declaration of Helsinki and approved by the local ethics committee of Xi'an Central Hospital affiliated with Xi'an Jiaotong University.

Subjects

Forty full-time welders and thirty-five HCs were enrolled in this study. Each patient met the inclusion criteria as follows: (i) having more than 5 years of welding experience in factories; (ii) being over 40 years old; (iii) having long-term accumulative effect of Mn and being chronically exposed to Mn. All HCs met the inclusion criteria as follows: (i) age- and gender-matching with the patients; (ii) not being exposed to either other hazardous materials or Mn.

All subjects were excluded from this study if he/she met any of these criteria as follows: (i) being left-handed; (ii) having a history of brain surgery, head injury and other psychiatric diseases; (iii) being addicted to alcohol, nicotine, or drug; (iv) being pregnant or lactating; (v) having any MRI contraindications. We conducted a questionnaire, urinary sample for Mn and brain MRI scanning for each subject on the same day.

MRI data acquisition

Each subject underwent MRI scanning with a 3.0-T MR system (Philips Ingenia) at the MR Research Center, Xi'an Central

Hospital, Shaanxi, China. High-resolution T1-weighted images were acquired using a 3D fast-spoiled gradient-echo sequence with the following parameters: repetition time = 6.6 ms, echo time = 3 ms, flip angle = 8°, field of view = 240 × 240 mm^2, matrix size = 240 × 240, resolution = 1.0 × 1.0 × 1.0 mm^3, slice thickness = 1 mm, 150 slices, no gap. In order to reduce scanner noise and minimize head movements, a standard bird-cage head coil was applied with foam pillows filling around each subject's head. During the scanning, each subject was instructed to keep their eyes closed and to stay awake without thinking anything.

MRI data preprocessing

Based on the platform of MATLAB 2014 (Matrix & Laboratory), structural image preprocessing and analysis were performed in the Computational Anatomy Toolbox 12 [18] (CAT12, http://dbm.neuro.uni-jena.de/cat/) implemented within Statistical Parametric Mapping 12 [19] (SPM12, http://www.fil.ion.ucl.ac.uk/spm/software/spm12/).

Firstly, brain images were segmented into gray matter, white matter, and cerebrospinal fluid by tissue probabilistic maps. Secondly, brain images were registered to the Montreal Neurological Institute (MNI) space and spatially normalized using Diffeomorphic Anatomical Registration Through Exponentiated Lie Algebra algorithm [20]. The resultant images in MNI space were modulated by the Jacobian determinants [21]. Finally, images were smoothed through a Gaussian kernel of 8 mm full-width at half maximum [19]. During the preprocessing on CAT12, total intracranial volume, GMV, white matter volume, and cerebrospinal fluid of the whole brain were calculated based on the segment maps. In order to optimize image quality before further analysis, each gray matter image was visually inspected. Images with poor quality were excluded from subsequent analysis.

Statistical analysis

Group differences of the demographic and clinical characteristics were computed by SPSS 23.0 (IBM). The results were expressed as mean ± standard deviation.

A two-sample t-test was performed to generate the VBM group statistical parametric maps in the whole brain, including age, gender, and total intracranial volume as covariates of no interest with false discovery rate (FDR) correction. Regions revealing significant differences, based on the statistic parametric maps, were selected as ROIs with a 3-mm radius sphere centered at the MNI coordinates of the peak t value for subsequent analysis.

The receiver operating characteristic (ROC) curve method was applied to examine the specificity and sensitivity of the ROIs-related abnormalities in GMV, which enabled the assessment of the discriminative power of the observed GMV changes in ROIs in identifying the patients. In addition, a nonparametric permutation test (5000 permutations) was used to exclude the possibility of the ROC results occurred by chance.

Multiple regression analysis was applied to investigate distinct ROI-related whole-brain voxel-wise structural covariance patterns in HCs and patient groups. The mean GMV of each ROI was included as a regressor in the regression model, and the total intracranial volume, gender, and age were deemed as covariates of no interest. One sample *t* test was performed to establish structural covariance maps which showed positive covariance with the GMV of each ROI in each group. Our study only focused on the positive covariance of the ROIs with the other regions [22].

Pearson's correlation analysis was used to assess the correlations between the VBM-related findings and duration of exposure and urinary Mn levels in Mn-exposed welders with Bonferroni correction. FDR and Bonferroni correction were employed for multiple comparison corrections in the statistical analysis, and the significant thresholds were all set at $p < 0.05$. The specific image processing process was shown in Fig. S1 in the supplemental material.

Results

Demographics and clinical characteristics

Results of the demographics and characteristics in Mn-exposed welders and HCs group are summarized in Table 1.

Table 1 Demographics and clinical characteristics of the Mn-exposed welders and HCs

	HCs (n = 35)	Welders (n = 40)	p value
Age (years)	45.33 ± 3.24	46.35 ± 4.76	0.317[a]
Gender (male/female)	34/1	38/2	1.000[b]
Urinary Mn level (ug/L)	-	13.68 ± 1.20	-
Duration of exposure (years)	-	16.70 ± 5.97	-
Total intracranial volume	1618.22 ± 115.99	1520.23 ± 116.42	0.0008 [a]

HCs, healthy controls; *Mn*, manganese. Data were expressed as the mean ± standard deviation.

[a] represented the p value was calculated by a two-tailed two-sample t test,

[b] represented the p value was calculated by a two-tailed chi-square test (Yates' correction)

There were no significant differences in age and gender among the HCs and Mn-exposed welders ($p > 0.05$).

GMV results

As shown in Fig. 1, Mn-exposed welders exhibited significantly increased GMV in the bilateral medial prefrontal cortex (MPFC), brainstem, and right precentral gyrus compared to HCs. Clusters showing decreased GMV in Mn-exposed welders compared to HCs located in the bilateral hippocampus, parahippocampus, and lentiform nuclei (including the pallidum and putamen). The regions showing significant differences were selected as ROIs for subsequent analysis.

The ROC results indicated that the GMV in specific regions might potentially be deemed as biomarkers to distinguish welders with Mn exposure from HCs (Fig. 2). The left hippocampus/parahippocampus showed an area under the ROC curve (AUC) of 0.951 with a 95% confidence interval (CI) from 0.901 to 1.000. The right hippocampus/parahippocampus exhibited an AUC of 0.948 with 95% CI from 0.891 to 1.000. The AUC value in the left putamen was 0.938 (95% CI: 0.885–0.991). The AUC value in the right putamen was 0.909 (95% CI: 0.842–0.976).

Structural covariance results

We selected the brain regions showing the first two AUC mean values as ROIs for structural covariance analysis. The intergroup differences in structural covariance patterns related to the bilateral hippocampus/parahippocampus and putamen were shown in Fig. 3 and 4. Specifically, for the left hippocampus/parahippocampus ROI, structural covariance patterns with the bilateral caudate, thalamus, and left lentiform nucleus were shown in HCs, whereas right precuneus and left supplemental motor area (SMA) were found in Mn-exposed welders. For the right hippocampus/parahippocampus ROI, HCs exhibited structural covariance patterns with the bilateral thalamus, amygdala, precuneus, and left middle temporal gyrus (MTG), while Mn-exposed welders showed structural covariance patterns associated with the bilateral insula, middle cingulate cortex, and MTG. In addition, the right hippocampus/parahippocampus ROI and right SMA, as well

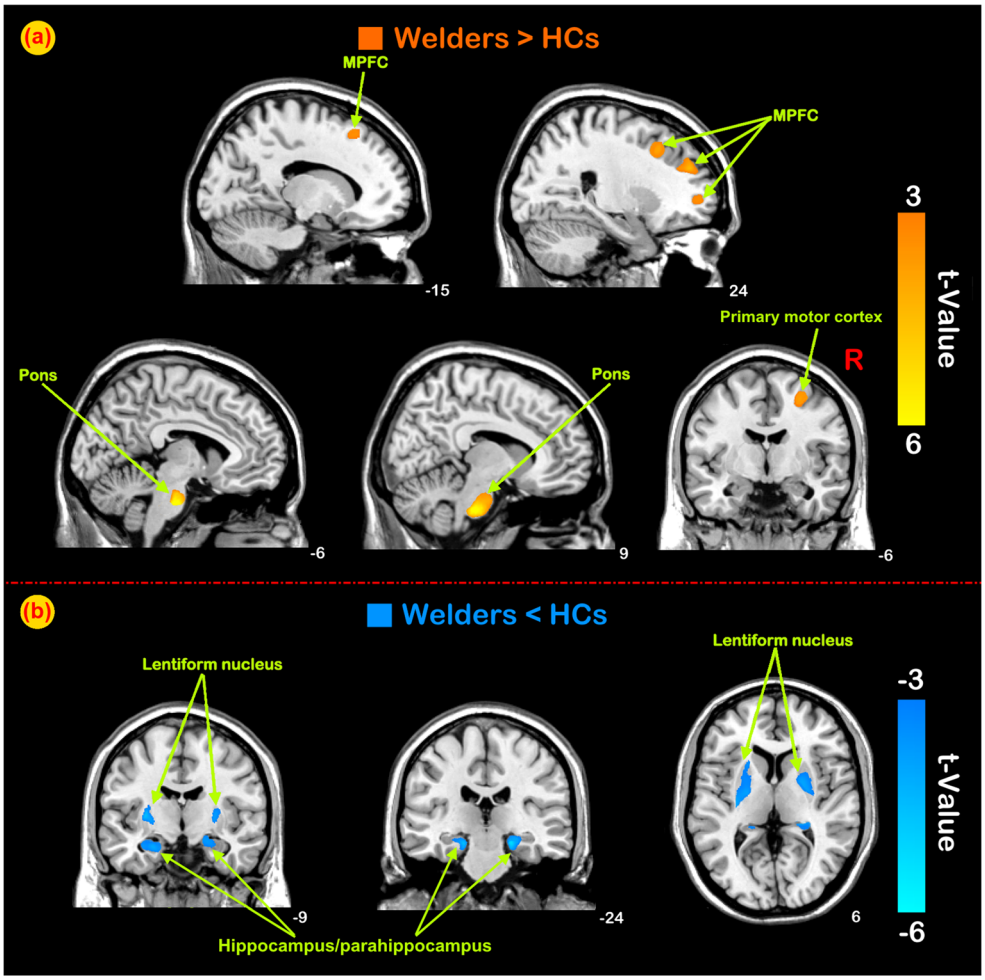

Fig. 1 Brain regions showing significant GMV changes in Mn-exposed welders compared to HCs. The warm color denotes significantly increased GMV (**a**), and the cool color denotes significantly decreased GMV (**b**)

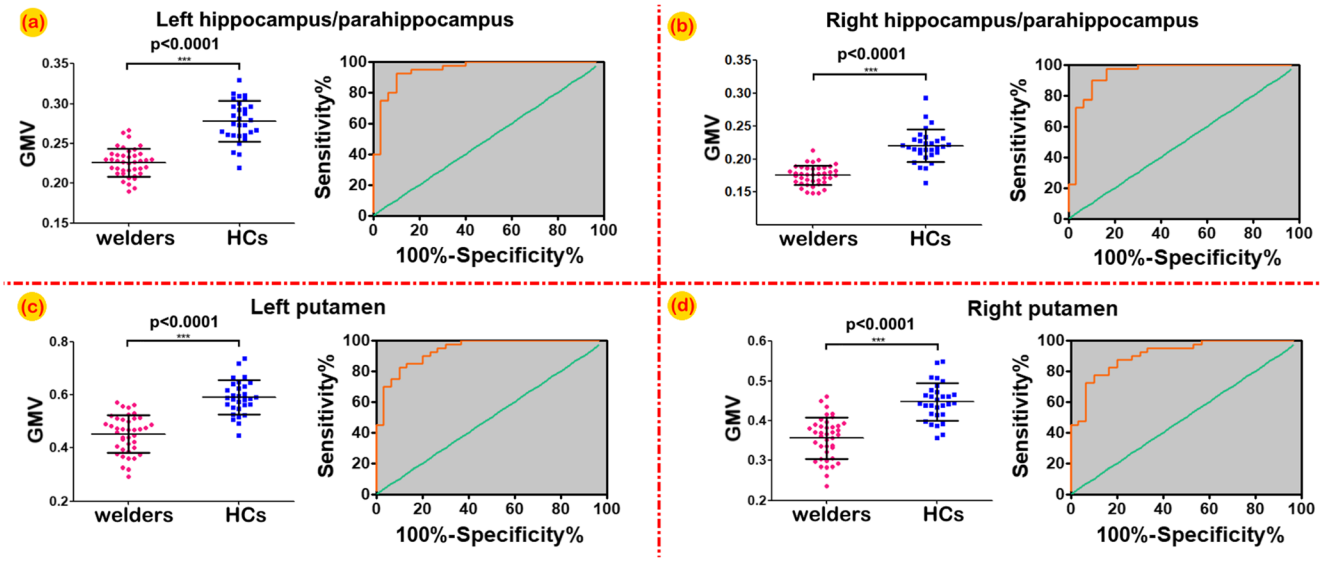

Fig. 2 Based on receiver operating characteristic (ROC) curve analysis, ROIs differentiating Mn-exposed welders from HCs by GMV in the left hippocampus/parahippocampus (**a**), right hippocampus/parahippocampus (**b**), left putamen (**c**), right putamen (**d**)

as middle cingulate cortex, in HCs were less spatially extended than those in Mn-exposed welders. The structural covariance patterns between the left putamen ROI and bilateral lentiform nucleus as well as MTG were detected in HCs, whereas patterns between the ROI and bilateral caudate and insula were only found in Mn-exposed welders. For the right putamen ROI, structural covariance connecting to the bilateral primary motor cortex, MTG, right caudate, and thalamus was displayed in HCs, while structural covariance connecting to the left primary motor cortex, bilateral caudate, insula, and several limbic regions including the bilateral hippocampus and amygdala was detected in Mn-exposed welders.

Correlation results

We found no significant relationships between the GMV findings and urinary Mn levels, as well as the duration of Mn exposure. However, the correlation analysis revealed linear declining trends of ROIs-related GMV values indices with the duration of Mn exposure.

Discussion

In the present study, morphometric brain alterations were examined in Mn-exposed welders based on the VBM and structural covariance analysis. Compared with HCs, Mn-exposed welders exhibited altered GMV in regions mainly including MPFC, primary motor cortex, hippocampus/parahippocampus, and lentiform nucleus. In addition, the hippocampus/parahippocampus exhibited the highest discrimination ability in ROC analysis than other brain regions showing different GMV between groups. For structural covariance analysis, distinct patterns were investigated between the ROIs and regions mainly encompassing the caudate, thalamus, insula, amygdala, SMA, primary motor cortex, and MTG.

Increased GMV in Mn-exposed welders

Our study applied VBM analysis and found that Mn-exposed welders had increased GMV in the bilateral MPFC compared to HCs. As a component of the executive control network, the MPFC is included in the inhibition motor system and plays a crucial role in modulating excessive limbic activity [23, 24]. For instance, Liao et al revealed that patients with a social anxiety disorder had increased GMV in the right MPFC, indicating the abnormalities might be associated with sustained and progressive inhibiting and modulating excessive limbic activity [25]. It has been revealed that the brain has the capacity to reserve or buffer, which enables it to resiliently deal with pathological attacks caused by disorders and aging [26]. Atrophic GMV in the MPFC was implicated in various disorders, such as bipolar disorder, schizophrenia, and Parkinson's disease [27–29]. However, in the present study, Mn-exposed welders showed increased GMV in the MPFC, and we speculated that there might present an appearance of expansion in the early stage and atrophy in the advanced stage as the disease progressed. Further investigations based on longitudinal data will be needed to refine our findings.

Neuropathological and neurodegenerative alterations in manganese toxicity are confined mainly to the striatum, pallidum, substantia nigra, and subthalamic nucleus [30]. In the present study, compared with HCs, Mn-exposed welders had significantly reduced GMV in the bilateral lentiform nucleus, hippocampus, and parahippocampus. The lentiform nucleus is composed of bilateral putamen and pallidum, which

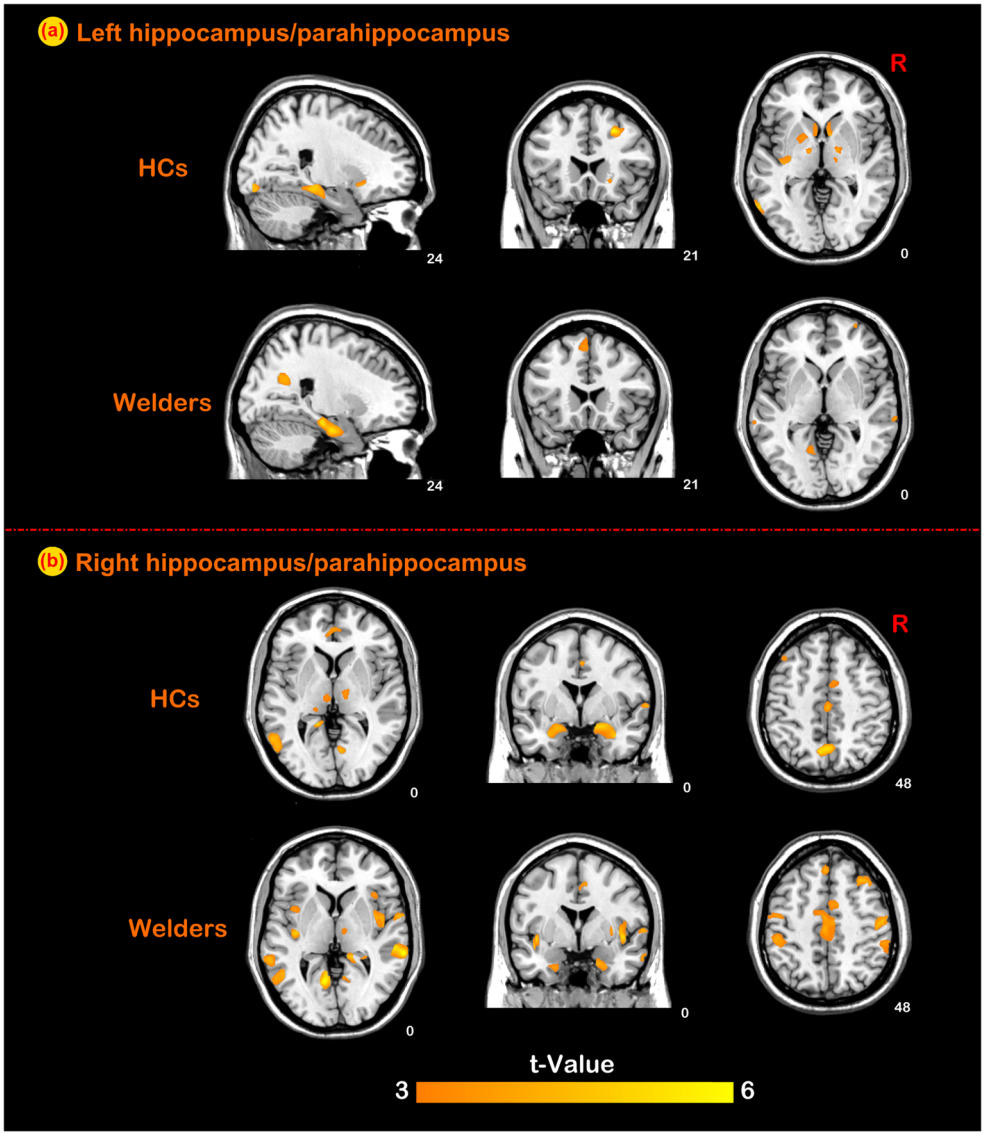

Fig. 3 Brain regions showing distinct left hippocampus/parahippocampus ROI (**a**) and right hippocampus/parahippocampus ROI (**b**)-based structural covariance patterns in both Mn-exposed welders and HCs

are also crucial components of the basal ganglia. The basal ganglia is a complex group of interconnected subcortical structures, which principally participated in sensorimotor control, cognitive functions, motivated behavior, and limbic control [31]. The basal ganglia was considered the primary target of Mn accumulation in the brain, and dysfunctions of the basal ganglia motor circuit have gradually become the focus on Mn toxicity mechanisms-related studies [32, 33]. Anatomical inputs from the motor cortex and substantia nigra are received by the striatum and transmitted via the pallidum, forming programming motor circuits [34]. Patients with Parkinsonism revealed progressive atrophy of basal ganglia based on susceptibility-weighted imaging, and the radiomics features derived from the putamen exhibited the best performance in differentiating idiopathic Parkinson's disease from other forms of Parkinsonism [35]. In addition, it has been reported that adults with Mn intoxication showed decreased white matter integrity and GMV. For example, in a diffusion-weighted imaging study, diffusion coefficient values, notably the putamen and pallidum, were detected to be reduced apparently in Mn-exposed welders [36]. Chang et al investigated occupationally Mn-exposed welders had significantly decreased GMV in the pallidum based on the whole brain VBM analysis [37]. Hence, reduced GMV in the putamen as well as pallidum might be associated with disturbances in motor control, and the ROC results of altered GMV in the putamen might serve as a potential biomarker for Mn overexposure. The hippocampus/parahippocampus are temporal brain structures and have fundamental roles in learning, memory processing, and emotional regulating [38]. Mn-exposed nonhuman primates revealed increased Mn concentrations in the hippocampus [39]. Moreover, previous imaging studies reported that hippocampal atrophy in the brain was associated with neurodegenerative diseases, such as Parkinson's disease

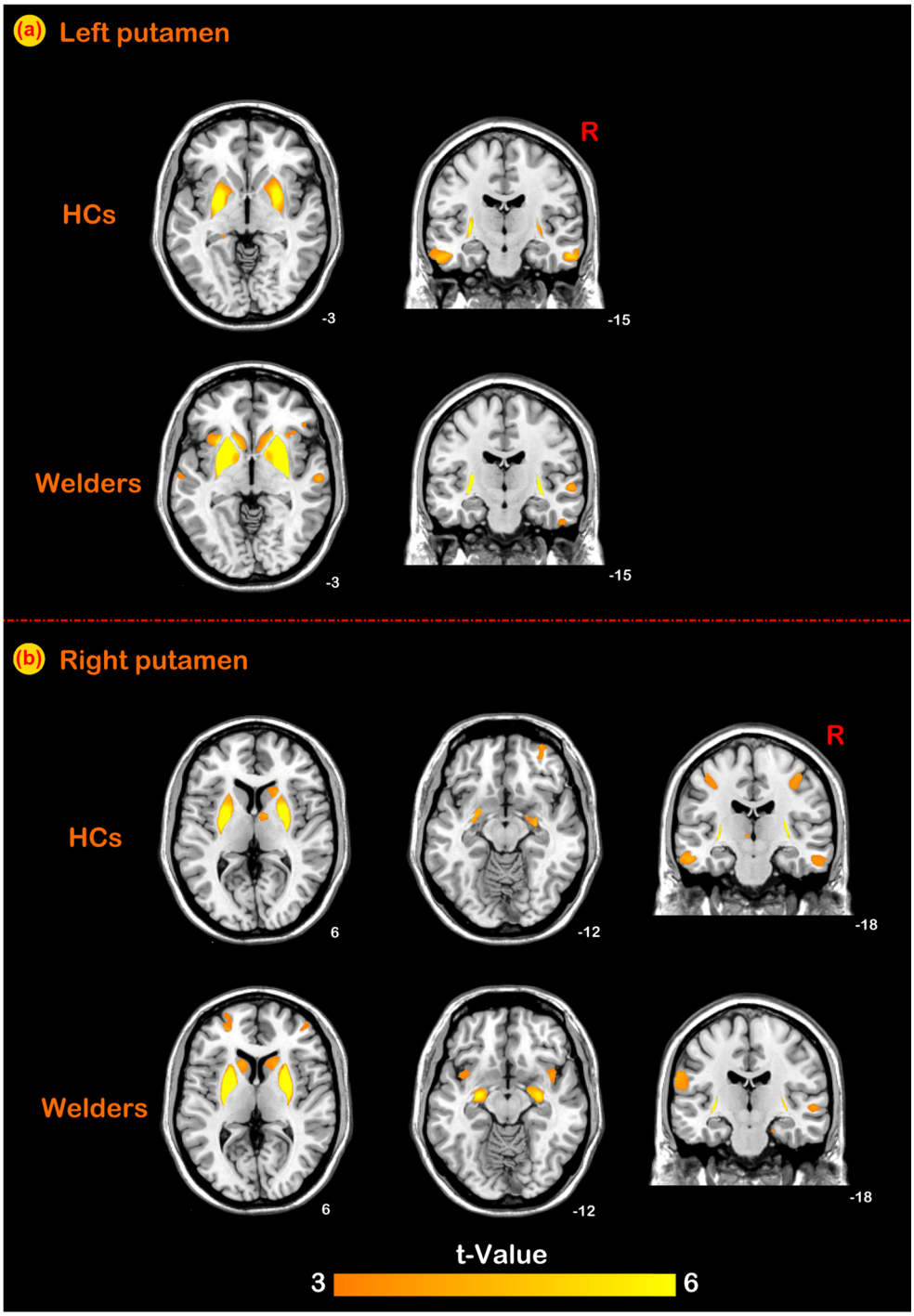

Fig. 4 Brain regions showing distinct left putamen ROI (**a**) and right putamen ROI (**b**)-based structural covariance patterns in both Mn-exposed welders and HCs

[40–42]. Therefore, our current findings combined with recent Mn-related neurotoxicity results indicated that reduced GMV in the hippocampus/parahippocampus might be implicated in neurodegeneration and cognitive impairment in Mn-exposed welders.

One major finding in this study was that structural covariance patterns of the ROIs were mainly located in SMA, insula, and MTG in Mn-exposed welders. The SMA is contributed to sensory and motor coordinative control [43]. The SMA connects the motor and limbic systems and transforms the negative emotional experience into protective motor behavior [44, 45]. A neurobehavior test observed that compared to HCs, SMA was hyperactivity in Mn-exposed welders with subclinical motor deficits [7]. Taken together, abnormal structural associations between the ROIs and motor cortex might bias Mn-exposed welders and suggest a compensatory strategy implicated in motor control and modulation. The insula has emerged as a major hub within the salient network and limbic

circuit and is related to somatomotor, as well as cognitive-evaluative and affective-perceptual forms of empathy [46]. Indeed, morphological and FC studies noted that motor and cognition-related diseases were implicated in abnormalities of the insula [47–49]. Consequently, the increased structural covariance between the ROIs and bilateral insula possibly suggested enhanced sensitivity to interoception of physiological processing and autonomic movement. The MTG is a component of the central sympathetic system and contributes to executive and cognitive functions including semantic processing. Several studies observed that patients with neurodegenerative diseases had atrophic GMV in the MTG [50, 51]. The stronger structural covariance probably reveals synchronous GMV changes in brain regions implicated in the diseases [11]. Hence, we suggested that the altered structural covariance between the ROIs and MTG might indicate synchronous atrophy in the Mn-exposed welder group. Taken together, our findings of increased structural covariance in these brain regions might imply reorganization mechanisms associated with cognitive and motivative processing.

Moreover, the HCs group exhibited increased structural covariance between the ROIs and thalamus in this study. Located in the diencephalon, the thalamus is a key relay hub of the thalamocortical loop and is involved in multiple functions including cognitive control, attentional processing, and emotional modulation [52]. Abnormalities in the thalamus were closely correlated with cognitive and emotional disorders [53–56]. Neuroimaging studies exhibited patients with Parkinsonism had GMV atrophy in the thalamus [57, 58]. Therefore, the lack of structural covariance between the ROIs and thalamus might be linked to the weaker cognitive and emotional information communication as well as dysfunction of homeostatic afferent in welders.

Several limitations should be noted in the present study. Firstly, the sample size in the current study was relatively small, and further studies with an expanded clinical dataset might validate our findings. Secondly, this study was limited by the lack of neurobehavioral data and clinical information on Mn-exposed welders, and more detailed clinical data would be needed to help validate our findings. Thirdly, our cross-sectional study did not observe correlations between altered GMV and characteristics, and a longitudinal study might help us to refine our findings.

In summary, this investigation found that Mn-exposed welders had morphological changes in brain structures mainly including MPFC, hippocampus, parahippocampus, and lentiform nucleus, compared to HCs. The significantly structural changes in the hippocampus/parahippocampus and putamen might be partly served as potential biomarkers for Mn overexposure. The distinct structural covariance patterns in the two groups of aforementioned regions were associated with the thalamus, insula, amygdala, SMA, and MTG, which were implicated in emotional modulation, cognitive control, and motor-related response. We hope the current study will provide a new perspective and neuroimaging evidence on potential neural mechanisms of Mn overexposure.

Supplementary Information The online version contains supplementary material available at https://doi.org/10.1007/s00330-022-08908-y.

Acknowledgements We would like to thank all subjects and foundation grant recipients in our study. We also thank the anonymous reviewers for their helpful suggestions and comments on the earlier version of our manuscript.

Funding This study has received funding from Xi'an Health Commission Science Foundation (No.2022qn03), Xi'an Central Hospital Science Foundation (No.2022QN05, 2022ZD01), the National Natural Science Foundation of China (No. 81771918), and Shaanxi National Science Foundation (No.2020JM-197, 2021JZ-58).

Declarations

Guarantor The scientific guarantor of this publication is Xiaoping Wu.

Conflict of interest The authors of this manuscript declare no relationships with any companies, whose products or services may be related to the subject matter of the article.

Statistics and biometry No complex statistical methods were necessary for this paper.

Informed consent Written informed consent was obtained from all subjects (patients) in this study.

Ethical approval Institutional Review Board approval was obtained.

Methodology
- prospective
- cross-sectional study
- performed at one institution

References

1. Miah MR, Ijomone OM, Okoh CO et al (2020) The effects of manganese overexposure on brain health. Neurochem Int 135: 104688
2. Dobson AW, Erikson KM, Aschner M (2004) Manganese neurotoxicity. Ann N Y Acad Sci 1012:115–128
3. Chang Y, Lee JJ, Seo JH et al (2010) Altered working memory process in the manganese-exposed brain. NeuroImage 53:1279–1285
4. Guilarte TR (2010) Manganese and Parkinson's disease: a critical review and new findings. Environ Health Perspect 118:1071–1080
5. Lee EY, Flynn MR, Du G et al (2019) Higher hippocampal mean diffusivity values in asymptomatic welders. Toxicol Sci 168:486–496
6. Kim Y, Jeong K, Song H et al (2011) Altered white matter microstructural integrity revealed by voxel-wise analysis of diffusion tensor imaging in welders with manganese exposure. Neurotoxicology 32:100–109
7. Chang Y, Song HJ, Lee JJ et al (2010) Neuroplastic changes within the brains of manganese-exposed welders: recruiting additional neural resources for successful motor performance. Occup Environ Med 67:809–815

8. Donzuso G, Sciacca G, Rascuna C et al (2021) Structural MRI substrate of long-duration response to levodopa in Parkinson's disease: an exploratory study. J Neurol 268:4258–4264
9. Samuraki M, Matsunari I, Yoshita M et al (2015) Cerebral amyloid angiopathy-related microbleeds correlate with glucose metabolism and brain volume in Alzheimer's disease. J Alzheimers Dis 48:517–528
10. Jayarajan RN, Agarwal SM, Viswanath B et al (2015) A voxel based morphometry study of brain gray matter volumes in juvenile obsessive compulsive disorder. J Can Acad Child Adolesc Psychiatry 24:84–91
11. Alexander-Bloch A, Giedd JN, Bullmore E (2013) Imaging structural co-variance between human brain regions. Nat Rev Neurosci 14:322–336
12. Ashburner J, Friston KJ (2000) Voxel-based morphometry–the methods. NeuroImage 11:805-821
13. Yee Y, Fernandes DJ, French L et al (2018) Structural covariance of brain region volumes is associated with both structural connectivity and transcriptomic similarity. NeuroImage 179:357–372
14. Wang Y, Yang Z, Wang Y et al (2020) Grey matter volume and structural covariance associated with schizotypy. Schizophr Res 224:88–94
15. Zhou C, Gao T, Guo T et al (2020) Structural covariance network disruption and functional compensation in Parkinson's disease. Front Aging Neurosci 12:199
16. Wu J, Gao M, Piao R, Feng N, Geng B, Liu P (2021) Magnetic resonance imaging-based structural covariance changes of the striatum in lifelong premature ejaculation patients. J Magn Reson Imaging 55:443–450
17. Zhang S, Chen F, Wu J et al (2021) Regional gray matter volume changes in brains of patients with ulcerative colitis. Inflamm Bowel Dis. https://doi.org/10.1093/ibd/izab252
18. Dahnke R, Yotter RA, Gaser C (2013) Cortical thickness and central surface estimation. NeuroImage 65:336–348
19. Kurth F, Gaser C, Luders E (2015) A 12-step user guide for analyzing voxel-wise gray matter asymmetries in statistical parametric mapping (SPM). Nat Protoc 10:293–304
20. Ashburner J (2007) A fast diffeomorphic image registration algorithm. NeuroImage 38:95–113
21. Good CD, Johnsrude IS, Ashburner J, Henson RN, Friston KJ, Frackowiak RS (2001) A voxel-based morphometric study of ageing in 465 normal adult human brains. NeuroImage 14:21–36
22. Seeley WW, Crawford RK, Zhou J, Miller BL, Greicius MD (2009) Neurodegenerative diseases target large-scale human brain networks. Neuron 62:42–52
23. Warwick JM, Carey P, Jordaan GP, Dupont P, Stein DJ (2008) Resting brain perfusion in social anxiety disorder: a voxel-wise whole brain comparison with healthy control subjects. Prog Neuropsychopharmacol Biol Psychiatry 32:1251–1256
24. Aron AR, Poldrack RA (2006) Cortical and subcortical contributions to stop signal response inhibition: role of the subthalamic nucleus. J Neurosci 26:2424–2433
25. Liao W, Xu Q, Mantini D et al (2011) Altered gray matter morphometry and resting-state functional and structural connectivity in social anxiety disorder. Brain Res 1388:167–177
26. Staff RT (2012) Reserve, brain changes, and decline. Neuroimaging Clin N Am 22:99–105
27. Zhao Y, Wang L, Edmiston EK et al (2021) Alterations in gray matter volumes and intrinsic activity in the prefrontal cortex are associated with suicide attempts in patients with bipolar disorder. Psychiatry Res Neuroimaging 307:111229
28. Jiang Y, Duan M, Chen X et al (2019) Aberrant prefrontal-thalamic-cerebellar circuit in schizophrenia and depression: evidence from a possible causal connectivity. Int J Neural Syst 29: 1850032
29. Cardoso EF, Maia FM, Fregni F et al (2009) Depression in Parkinson's disease: convergence from voxel-based morphometry and functional magnetic resonance imaging in the limbic thalamus. NeuroImage 47:467–472
30. Aschner M, Erikson KM, Herrero Hernandez E, Tjalkens R (2009) Manganese and its role in Parkinson's disease: from transport to neuropathology. Neuromolecular Med 11:252–266
31. Alexander GE, DeLong MR, Strick PL (1986) Parallel organization of functionally segregated circuits linking basal ganglia and cortex. Annu Rev Neurosci 9:357–381
32. Crossgrove J, Zheng W (2004) Manganese toxicity upon overexposure. NMR Biomed 17:544–553
33. Criswell SR, Perlmutter JS, Videen TO et al (2011) Reduced uptake of [(1)(8)F]FDOPA PET in asymptomatic welders with occupational manganese exposure. Neurology 76:1296–1301
34. Lao Y, Dion LA, Gilbert G et al (2017) Mapping the basal ganglia alterations in children chronically exposed to manganese. Sci Rep 7:41804
35. Pang H, Yu Z, Li R, Yang H, Fan G (2020) MRI-based radiomics of basal nuclei in differentiating idiopathic Parkinson's disease from parkinsonian variants of multiple system atrophy: a susceptibility-weighted imaging study. Front Aging Neurosci 12:587250
36. Criswell SR, Perlmutter JS, Huang JL et al (2012) Basal ganglia intensity indices and diffusion weighted imaging in manganese-exposed welders. Occup Environ Med 69:437–443
37. Chang Y, Jin SU, Kim Y et al (2013) Decreased brain volumes in manganese-exposed welders. Neurotoxicology 37:182–189
38. Bartsch T, Wulff P (2015) The hippocampus in aging and disease: from plasticity to vulnerability. Neuroscience 309:1–16
39. Dorman DC, Struve MF, Marshall MW, Parkinson CU, James RA, Wong BA (2006) Tissue manganese concentrations in young male rhesus monkeys following subchronic manganese sulfate inhalation. Toxicol Sci 92:201–210
40. Chapleau M, Aldebert J, Montembeault M, Brambati SM (2016) Atrophy in alzheimer's disease and semantic dementia: an ale meta-analysis of voxel-based morphometry studies. J Alzheimers Dis 54: 941–955
41. Xu Y, Yang J, Hu X, Shang H (2016) Voxel-based meta-analysis of gray matter volume reductions associated with cognitive impairment in Parkinson's disease. J Neurol 263:1178–1187
42. Zackova L, Jani M, Brazdil M, Nikolova YS, Mareckova K (2021) Cognitive impairment and depression: meta-analysis of structural magnetic resonance imaging studies. NeuroImage Clin 32:102830
43. Wang S, Zhang Y, Lei J, Guo S (2021) Investigation of sensorimotor dysfunction in Parkinson disease by resting-state fMRI. Neurosci Lett 742:135512
44. Pawliczek CM, Derntl B, Kellermann T, Kohn N, Gur RC, Habel U (2013) Inhibitory control and trait aggression: neural and behavioral insights using the emotional stop signal task. NeuroImage 79:264–274
45. Sagaspe P, Schwartz S, Vuilleumier P (2011) Fear and stop: a role for the amygdala in motor inhibition by emotional signals. NeuroImage 55:1825–1835
46. Uddin LQ, Nomi JS, Hebert-Seropian B, Ghaziri J, Boucher O (2017) Structure and function of the human insula. J Clin Neurophysiol 34:300–306
47. Etkin A, Wager TD (2007) Functional neuroimaging of anxiety: a meta-analysis of emotional processing in PTSD, social anxiety disorder, and specific phobia. Am J Psychiatry 164:1476–1488
48. Geng B, Gao M, Wu J et al (2021) Smaller volume and altered functional connectivity of the amygdala in patients with lifelong premature ejaculation. Eur Radiol 31:8429–8437
49. Jonkman LE, Fathy YY, Berendse HW, Schoonheim MM, van de Berg WD (2021) Structural network topology and microstructural alterations of the anterior insula associate with cognitive and affective impairment in Parkinson's disease. Sci Rep 11:16021

50. Whitwell JL, Shiung MM, Przybelski SA et al (2008) MRI patterns of atrophy associated with progression to AD in amnestic mild cognitive impairment. Neurology 70:512–520
51. Duara R, Loewenstein DA, Potter E et al (2008) Medial temporal lobe atrophy on MRI scans and the diagnosis of Alzheimer disease. Neurology 71:1986–1992
52. Arend I, Henik A, Okon-Singer H (2015) Dissociating emotion and attention functions in the pulvinar nucleus of the thalamus. Neuropsychology 29:191–196
53. Li R, Zou T, Wang X et al (2022) Basal ganglia atrophy-associated causal structural network degeneration in Parkinson's disease. Hum Brain Mapp 43:1145–1156
54. van de Mortel LA, Thomas RM, van Wingen GA, Alzheimer's Disease Neuroimaging Initiative (2021) Grey Matter loss at different stages of cognitive decline: a role for the thalamus in developing Alzheimer's disease. J Alzheimers Dis 83:705–720
55. Xiong G, Dong D, Cheng C et al (2021) Potential structural trait markers of depression in the form of alterations in the structures of subcortical nuclei and structural covariance network properties. NeuroImage Clin 32:102871
56. Heitmann CY, Feldker K, Neumeister P et al (2016) Abnormal brain activation and connectivity to standardized disorder-related visual scenes in social anxiety disorder. Hum Brain Mapp 37: 1559–1572
57. Zarkali A, McColgan P, Leyland LA, Lees AJ, Weil RS (2022) Longitudinal thalamic white and grey matter changes associated with visual hallucinations in Parkinson's disease. J Neurol Neurosurg Psychiatry 93:169–179
58. Li M, He J, Liu X, Wang Z, Lou X, Ma L (2020) Structural and functional thalamic changes in parkinson's disease with mild cognitive impairment. J Magn Reson Imaging 52:1207–1215